LETTERS
https://doi.org/10.1038/s41563-019-0294-7
nature materials

Nonlinear anomalous Hall effect in few-layer WTe_2

Kaifei Kang[1,5], Tingxin Li[1,5], Egon Sohn[2,3,5], Jie Shan[1,2,4*] and Kin Fai Mak[1,2,4*]

The Hall effect occurs only in systems with broken time-reversal symmetry, such as materials under an external magnetic field in the ordinary Hall effect and magnetic materials in the anomalous Hall effect (AHE)[1]. Here we show a nonlinear AHE in a non-magnetic material under zero magnetic field, in which the Hall voltage depends quadratically on the longitudinal current[2–6]. We observe the effect in few-layer T_d-WTe_2, a two-dimensional semimetal with broken inversion symmetry and only one mirror line in the crystal plane. Our angle-resolved electrical measurements reveal that the Hall voltage maximizes (vanishes) when the bias current is perpendicular (parallel) to the mirror line. The observed effect can be understood as an AHE induced by the bias current, which generates an out-of-plane magnetization. The temperature dependence of the Hall conductivity further suggests that both the intrinsic Berry curvature dipole and extrinsic spin-dependent scatterings contribute to the observed nonlinear AHE.

Unlike the linear Hall effect, which has to vanish to satisfy the Onsager reciprocity relation in a time-reversal invariant system, the nonlinear Hall effect, in principle, does not have to vanish[7]. On the other hand, a second-order nonlinear effect occurs only in systems with broken inversion symmetry[8]. Atomically thin T_d-WTe_2 possesses all the right symmetries to realize the second-order nonlinear Hall effect in the absence of an external magnetic field. The effect is referred to as a nonlinear anomalous Hall effect (AHE) in analogy to the AHE in magnetic materials since it originates from a sample magnetization rather than a Lorentz force induced by a magnetic field. Monolayer WTe_2 of the T_d/T' polytype consists of a layer of W atoms sandwiched between two layers of Te atoms in a distorted octahedral coordination[9] (Fig. 1a). It is centrosymmetric with one mirror line (dashed line, Fig. 1a) along the crystal b-axis. Multilayer T_d-WTe_2 is formed by stacking monolayers with alternating layers rotated by 180° (ref. [9]) (Fig. 1a). It is non-centrosymmetric and has point group Pm (ref. [10]). In contrast to the bulk (point group $Pmn2_1$)[9], the screw-axis and glide-plane symmetries are broken at the surfaces to allow an in-plane polar axis along the mirror line. Pristine T_d-WTe_2 is a semimetal with nearly compensated electron and hole densities down to a thickness of three layers[11–14]. An array of quantum revelations has been recently reported in this system, including a two-dimensional (2D) topological insulator in the monolayer limit[15–18], a switchable ferroelectric metal in two and three layers[19], superconductivity induced by electrostatic doping in monolayers[20,21], and a Berry curvature dipole effect in transport in gapped bilayer WTe_2 (ref. [22]). Here we investigate the nonlinear electrical properties of few-layer T_d-WTe_2, particularly in the metallic regime.

In our experiment, T_d-WTe_2 samples with a thickness of four to eight layers have been studied. Both the Hall bar and circular disc devices with electrodes aligned with the crystal axes were employed (Fig. 1b). The disc devices were essential for angle-resolved electrical measurements. (See Methods and Supplementary Section 1 for details of the sample and device fabrication.) Figure 1c,d shows the result of the basic electrical characterization of a typical Hall bar device. The temperature dependence of the longitudinal resistivity $\rho_\parallel$ along the crystal a-axis (Fig. 1c) shows a typical metallic behaviour below about 100 K with a residual resistivity of about 50 μΩ cm. Above 100 K, the dependence deviates from the linear relation, which is probably a manifestation of non-degenerate electron gases[14] (in semimetallic WTe_2, the electron and hole gases can be easily thermally excited because of the low densities). Figure 1d is the magnetic-field dependence of $\rho_\parallel$ (black line) and the transverse (Hall) resistivity $\rho_\perp$ (red line) at 1.8 K. The field is out of plane. The large non-saturating $\rho_\parallel$ up to 14 T indicates a nearly compensated electron and hole density[11,13,14]. $\rho_\perp$ depends approximately linearly on field. Shubnikov–de Haas oscillations start to emerge around 7 T, indicative of high sample quality. Using the two-carrier analysis of the magnetic-field dependence of $\rho_\parallel$ and $\rho_\perp$ (refs. [13,14,23]), we extract the carrier densities, about 1.26×10^{13} cm^{-2} (electron) and about 1.16×10^{13} cm^{-2} (hole), and mobilities, about 1580 cm^2 V^{-1} s^{-1} (electron) and about 960 cm^2 V^{-1} s^{-1} (hole). The mobilities along the crystal b-axis are typically two to three times smaller. The behaviour of other Hall bar devices (summarized in Supplementary Section 4) is similar. These results are consistent with the reported results[11,13,14,23].

To measure nonlinear transport in few-layer WTe_2, we bias the Hall bar device with a harmonic current along the a-axis at a fixed frequency (137 Hz) and record the longitudinal and transverse voltage drops at both the fundamental and second-harmonic frequencies. (See Methods for details of the electrical measurements.) The results are independent of driving frequency (Supplementary Section 3), which excludes potential measurement artifacts such as spurious capacitive coupling. Figure 2 is the result from a five-layer Hall bar device at 1.8 K under zero magnetic field. At the fundamental frequency (Fig. 2a), the longitudinal voltage $V_\parallel$ increases linearly with current I till sample heating becomes significant at large currents. The transverse voltage $V_\perp$ remains small (~1% of $V_\parallel$). The observed finite value of $V_\perp$ arises from misalignment of the electrodes with the crystal axes (typically of the order of ~1°) and the intrinsic resistance anisotropy of the material. The second-harmonic transverse response $V_\perp^{2\omega}$ (Fig. 2b) is approximately 0.1% of $V_\parallel$ at high bias voltages. It scales linearly with the square of the current, or equivalently $V_\parallel$. It switches sign when the current direction and the Hall probe connection are reversed simultaneously. Furthermore, very similar amplitude and bias current dependences have been observed for the d.c. (or rectification) component of the transverse voltage $V_\perp^{DC}$ (Fig. 2c for a four-layer device). All these results clearly indicate a second-order nonlinear charge response in few-layer WTe_2. Below we focus on $V_\perp^{2\omega}$.

We investigate $V_\perp^{2\omega}$ as a function of current direction. Disc devices (Fig. 1b) were utilized. Current I was injected through one

[1]School of Applied and Engineering Physics, Cornell University, Ithaca, NY, USA. [2]Laboratory of Atomic and Solid State Physics, Cornell University, Ithaca, NY, USA. [3]Department of Physics, Penn State University, University Park, PA, USA. [4]Kavli Institute at Cornell for Nanoscale Science, Ithaca, NY, USA. [5]These authors contributed equally: K. Kang, T. Li, E. Sohn. *e-mail: jie.shan@cornell.edu; kinfai.mak@cornell.edu

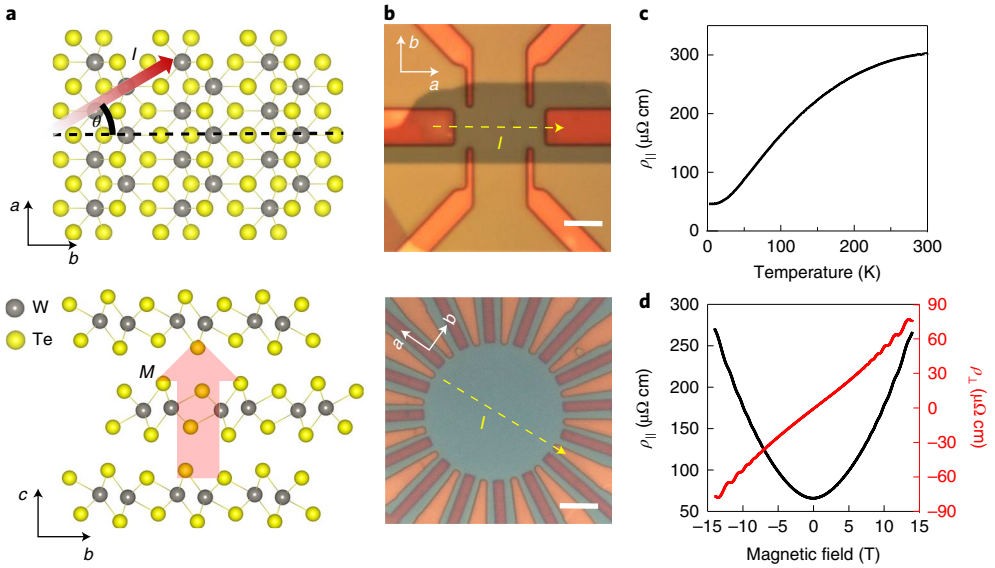

Fig. 1 | Atomic structure and basic characterization of few-layer WTe_2. a, *a*–*b* plane of monolayer and *b*–*c* plane of few-layer T_d-WTe_2. When an in-plane current *I* is biased at angle θ ($\neq$0) from the mirror line (dashed line), an out-of-plane magnetization (*M*) is generated. **b**, Optical image of a typical Hall bar (top) and a circular disc device used in this study (bottom). The scale bars are 5 μm. The crystal orientation was determined by polarized Raman spectroscopy. WTe_2 samples are in grey, Pt electrodes in orange and the Si substrate in dark red–orange for the disc device. Dashed yellow lines indicate the current direction. **c**,**d**, Temperature dependence of $\rho_{\parallel}$ (**c**) and magnetic-field dependence of $\rho_{\parallel}$ and $\rho_{\perp}$ (**d**) for a Hall bar device at 1.8 K.

of the 16 electrodes at angle θ from the mirror line (crystal *b*-axis), and the voltage drop across the electrodes along the diameter and perpendicular to the diameter were measured in a rotating reference frame. Results shown in Fig. 3 are from an eight-layer device. Consistent results were observed in all disc devices studied in this work (Supplementary Section 5). Again, the first-harmonic longitudinal and transverse voltages are linear with current. The slopes corresponding to the longitudinal and transverse resistances, $R_{\parallel}\left(\equiv\frac{V_{\parallel}}{I}\right)$ and $R_{\perp}\left(\equiv\frac{V_{\perp}}{I}\right)$, respectively, are presented in Fig. 3a as a function of θ. The second-harmonic transverse response is quadratic with $V_{\parallel}$ for all angles (Fig. 3b). The slope of $V_{\perp}^{2\omega}$ versus $(V_{\parallel})^2$ as a function of θ is summarized in Fig. 3c. The longitudinal and transverse resistances both show a two-fold angular dependence. This is consistent with the crystal symmetry of few-layer T_d-WTe_2 (ref. [10]) and can be expressed as $R_{\parallel}(\theta)=R_b\cos^2\theta+R_a\sin^2\theta$ and $R_{\perp}(\theta)=(R_b-R_a)\sin\theta\cos\theta$, where R_a and $R_b(>R_a)$ are the resistances along the crystal *a*- and *b*-axes, respectively. The fit (dashed lines, Fig. 3a) yields a resistance anisotropy $r\left(\equiv\frac{R_a}{R_b}\right)$ of about 0.3. This value is nearly temperature independent, particularly for temperatures below 100 K (Supplementary Section 2). In contrast, the nonlinear response shows a one-fold angular dependence. It reaches the maximum when the current is perpendicular to the mirror line (that is along the *a*-axis), and vanishes when the current is parallel to the mirror line (that is along the *b*-axis). We can express the nonlinear response through the second-order nonlinear susceptibilities (see Methods for derivation)

$$V_{\perp}^{2\omega}/(V_{\parallel})^2\propto\sin\theta\frac{d_{12}r^2\sin^2\theta+(d_{11}-2d_{26}r^2)\cos^2\theta}{(\cos^2\theta+r\sin^2\theta)^2} \quad (1)$$

where the d_{ij} are the non-vanishing elements of the second-order nonlinear susceptibility tensor for the *Pm* point group[8]. The overall $\sin\theta$ factor dictates that the effect is present only when there is a bias current component perpendicular to the mirror line. Equation (1) with three free parameters, including an overall amplitude, d_{12} and $d_{11}-2d_{26}r^2$, captures the experimental angular dependence of Fig. 3c very well (dashed line). The observed effect is fully consistent with a second-order nonlinear response to a bias current based on the symmetry of few-layer T_d-WTe_2 crystals.

Finally, we examine the microscopic mechanism of the observed nonlinear effect by studying its dependence on carrier scattering. We vary the scattering (or the material's conductivity) by changing the sample temperature (Fig. 4a). We focus on Hall bar devices, in which the crystals are aligned for the maximum nonlinear response. The Hall bar geometry also allows us to obtain the electric fields (and conductivities) from the voltage drops through the device dimensions, $E_{\perp}^{2\omega}\equiv\frac{V_{\perp}^{2\omega}}{L_{\perp}}$ and $E_{\parallel}\equiv\frac{V_{\parallel}}{L_{\parallel}}$, where $L_{\parallel}\approx6\,\mu$m and $L_{\perp}\approx9.2\,\mu$m are the longitudinal and transverse lengths of the Hall bar device, respectively. Similar to what has been observed at 1.8 K, $E_{\perp}^{2\omega}$ depends linearly on $(E_{\parallel})^2$ at all temperatures (Fig. 4b). The slope, however, decreases monotonically with increasing temperature. In Fig. 4c, we extract the slope for temperatures below 100 K, at which the electron and hole gases remain largely degenerate. Interestingly, the dependence resembles that of the longitudinal conductivity σ (Fig. 4a), which increases with decreasing temperature and saturates at a value limited by disorder scattering at low temperatures. A more careful analysis in Fig. 4d shows that $\frac{E_{\perp}^{2\omega}}{(E_{\parallel})^2}$ scales linearly with σ^2 (dashed line):

$$\frac{E_{\perp}^{2\omega}}{(E_{\parallel})^2}=\xi\sigma^2+\eta \quad (2)$$

where ξ and η are constants. This holds true for devices with nearly compensated electron and hole densities studied in this work.

The scaling result of equation (2) inferred from our experiment sheds light on the mechanism that gives rise to the second-order nonlinear response to current in few-layer T_d-WTe_2. We rewrite the left-hand side of equation (2) in terms of the conductivity ratio: $\frac{E_{\perp}^{2\omega}}{(E_{\parallel})^2}=\left(\frac{\sigma_{AH}}{r\sigma}\right)\frac{1}{E_{\parallel}}$, where the anomalous Hall conductivity σ_{AH} is

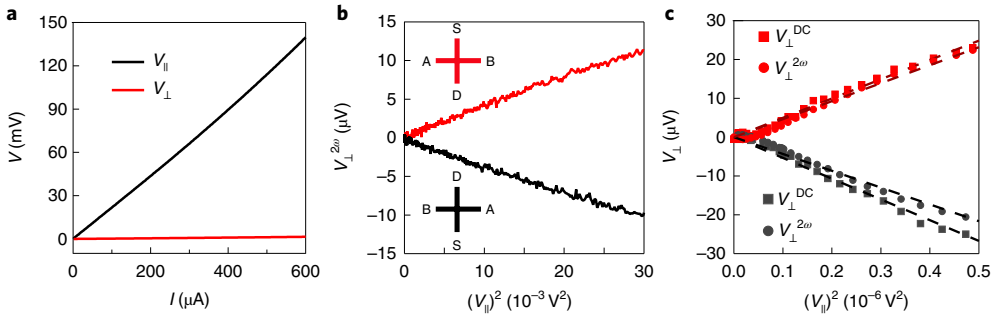

Fig. 2 | Nonlinear AHE. a, First-harmonic $V_\parallel$ and $V_\perp$ as a function of a.c. current amplitude I. Current is along the crystal a-axis. **b**, $V_\perp^{2\omega}$ depends linearly on the square of $V_\parallel$ and changes sign when the current direction reverses. The insets show the electrode geometry for the forward current (red) and backward current (black) directions. The current is injected from the source (S) to the drain (D) electrode and the voltage is measured between the A and B electrodes. **a** and **b** are results from a five-layer WTe_2 Hall bar device at 1.8 K under zero magnetic field. **c**, $V_\perp^{2\omega}$ and $V_\perp^{DC}$ as a function of $V_\parallel$ in a four-layer device under similar experimental conditions for the forward current (red symbols) and backward current (black symbols) directions. The uncertainties are smaller than the size of the symbols. The dashed lines are linear fits to experiment.

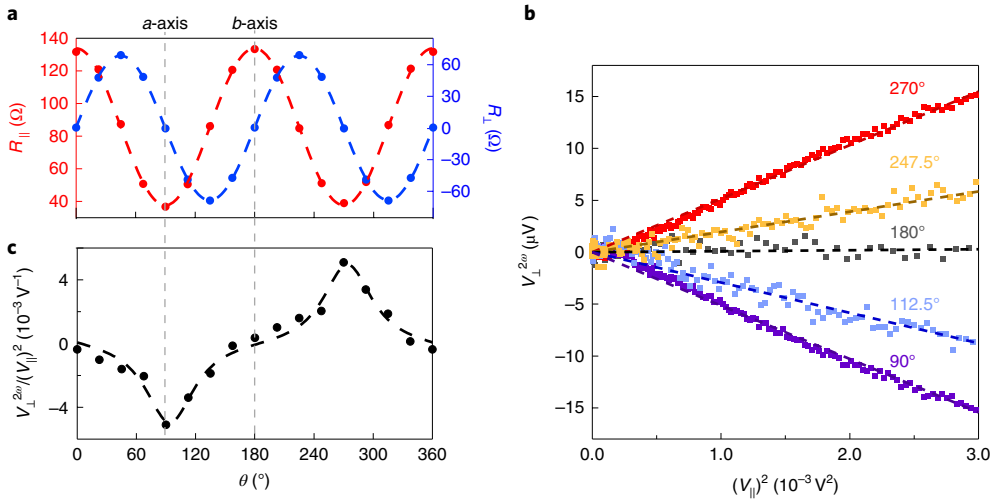

Fig. 3 | Angular dependence of the nonlinear AHE. a, $R_\parallel$ and $R_\perp$ of a disc device as a function of θ. **b**, $V_\perp^{2\omega}$ depends linearly on the square of the first-harmonic $V_\parallel$ for different current directions. **c**, The nonlinear Hall effect (slope of the dependences in **b**) as a function of θ. All measurements were performed at 1.8 K. The symbols in **a**, **b** and **c** are experimental data and the error bars are smaller than the size of the symbols. The dashed lines are fits to the experimental data with the model described in the main text.

the antisymmetric off-diagonal element of the conductivity tensor. σ_{AH} normalized by current density is a natural parameter for the second-order nonlinear AHE. Since σ depends linearly on scattering time τ (along the a-axis), equation (2) states that σ_{AH} has two contributions, which scale as τ^3 and τ, respectively. (Note that r is practically temperature independent within this temperature range.) This excludes effects, such as the ratchet effect from inversion asymmetric scattering, in which the transverse conductivity has been shown to scale as τ^2 (refs. [3,24,25]).

Our results are fully consistent with a current-induced AHE[3–6], in which an in-plane current generates an out-of-plane magnetization that acts as the spontaneous magnetization in the AHE in magnetic materials (Fig. 1a). In non-centrosymmetric metals with a polar axis such as T_d-WTe_2, a charge current creates a shift in the Fermi surface and perturbs the balance between the up and down magnetic moments[26]. The magnitude of the resultant magnetization is given by the dot product of the current and the Berry curvature dipole following Sodemann and Fu[3]. Such a current-induced magnetization has been observed in uniaxially strained monolayer MoS_2 using optical Kerr microscopy[27,28], and has been demonstrated as a spin source at the WTe_2/ferromagnet interfaces based on spin–orbit torque[29,30]. The current-induced magnetization scales as current, and thus τ. On the other hand, it is known that the AHE in magnetic materials can arise from both the intrinsic (Berry curvature) and extrinsic (spin-dependent scattering) effects[1]. When the sample temperature is varied, the anomalous Hall conductivity in magnetic materials has been shown to scale as τ^2 for the skew scattering contribution[31,32], and as τ^0 for the intrinsic and side-jump contributions[1]. Combining with the linear τ dependence of the current-induced magnetization, these effects fully account for the two terms in equation (2). If we neglect the side-jump contribution, we can further obtain an order of magnitude estimate of the Berry curvature dipole from the intersect η in equation (2). The range of η from our samples (with different doping densities, mobilities and sample thicknesses) is $\eta \approx (0.15–1) \times 10^{-3}\,\mu m\,V^{-1}$, corresponding to a Berry curvature dipole of $D \sim \eta^* \frac{\epsilon_F}{e} \sim$ 0.1–0.7 Å, where ϵ_F is the Fermi energy (see Methods). This value for the Berry curvature dipole is about two orders of magnitude larger than that predicted for monolayer MoS_2 under about 0.5% uniaxial strain[3,6,27]. The natural lattice distortion in T_d-WTe_2 endows the material with a much stronger Berry curvature dipole effect.

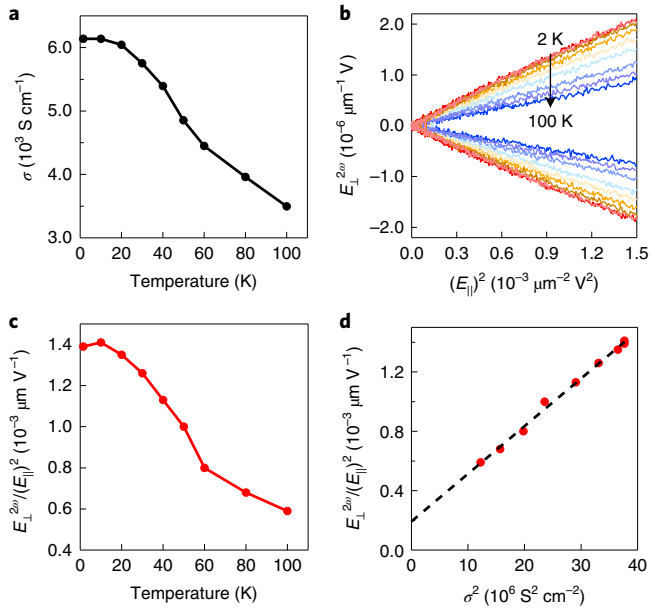

Fig. 4 | Temperature dependence of the nonlinear AHE. a, Temperature dependence of σ of the same Hall bar device as in Fig. 2a,b. **b**, $E_{\perp}^{2\omega}$ depends linearly on the square of $E_{\parallel}$ at temperatures ranging from 2 to 100 K (in the order 2, 10, 20, 30, 40, 50, 65, 80 and 100 K). It changes sign when the current direction reverses. **c**,**d**, The nonlinear Hall effect (slope of the dependences of **b**) as a function of temperature (**c**) and the square of the longitudinal conductivity (**d**). The symbols are experimental data with uncertainties smaller than the size the symbols. The lines in **a** and **c** are guides to the eye. The dashed line in **d** is a linear fit to the experimental data.

In conclusion, we have demonstrated a nonlinear Hall effect in non-magnetic few-layer T_d-WTe_2 under zero magnetic field through the angle-resolved electrical measurements. This is a universal phenomenon and only requires crystals with the right point group symmetry. The study indicates that both the intrinsic Berry curvature dipole and extrinsic spin-dependent scatterings contribute to the nonlinear Hall conductance in few-layer T_d-WTe_2. Our results open the possibility of exploring topological effects in solids by nonlinear electrical transport[3–6,33] and applications of the phenomenon in spin–orbit torque devices[29,30].

Online content

Any methods, additional references, Nature Research reporting summaries, source data, statements of data availability and associated accession codes are available at https://doi.org/10.1038/s41563-019-0294-7.

Received: 24 September 2018; Accepted: 22 January 2019;
Published online: 25 February 2019

References

1. Nagaosa, N., Sinova, J., Onoda, S., MacDonald, A. H. & Ong, N. P. Anomalous Hall effect. *Rev. Mod. Phys.* **82**, 1539–1592 (2010).
2. Low, T., Jiang, Y. & Guinea, F. Topological currents in black phosphorus with broken inversion symmetry. *Phys. Rev. B* **92**, 235447 (2015).
3. Sodemann, I. & Fu, L. Quantum nonlinear Hall effect induced by Berry curvature dipole in time-reversal invariant materials. *Phys. Rev. Lett.* **115**, 216806 (2015).
4. Zhang, Y., van den Brink, J., Felser, C. & Yan, B. Electrically tuneable nonlinear anomalous Hall effect in two-dimensional transition-metal dichalcogenides WTe_2 and $MoTe_2$. *2D Mater.* **5**, 044001 (2018).
5. Shi, L.-k. & Song, J. C. W. Symmetry, spin-texture, and tunable quantum geometry in a WTe_2 monolayer. *Phys. Rev. B* **99**, 035403 (2019).
6. You, J.-S., Fang, S., Xu, S.-Y., Kaxiras, E. & Low, T. Berry curvature dipole current in the transition metal dichalcogenides family. *Phys. Rev. B* **98**, 121109 (2018).
7. Landau, L. D., Lifshitz, E. M. & Pitaevskii, L. P. *Statistical Physics* (Pergamon, Oxford, 1999).
8. Shen, Y. R. *The Principles of Nonlinear Optics* (Wiley, Hoboken, 2002).
9. Brown, B. E. The crystal structures of WTe_2 and high-temperature $MoTe_2$. *Acta Crystallogr.* **20**, 268–274 (1966).
10. Song, Q. et al. The in-plane anisotropy of WTe_2 investigated by angle-dependent and polarized Raman spectroscopy. *Sci. Rep.* **6**, 29254 (2016).
11. Ali, M. N. et al. Large, non-saturating magnetoresistance in WTe_2. *Nature* **514**, 205–208 (2014).
12. Soluyanov, A. A. et al. Type-II Weyl semimetals. *Nature* **527**, 495–498 (2015).
13. Wang, Y. et al. Gate-tunable negative longitudinal magnetoresistance in the predicted type-II Weyl semimetal WTe_2. *Nat. Commun.* **7**, 13142 (2016).
14. Fatemi, V. et al. Magnetoresistance and quantum oscillations of an electrostatically tuned semimetal-to-metal transition in ultrathin WTe_2. *Phys. Rev. B* **95**, 041410 (2017).
15. Qian, X., Liu, J., Fu, L. & Li, J. Quantum spin Hall effect in two-dimensional transition metal dichalcogenides. *Science* **346**, 1344–1347 (2014).
16. Tang, S. et al. Quantum spin Hall state in monolayer 1T′-WTe_2. *Nat. Phys.* **13**, 683–687 (2017).
17. Fei, Z. et al. Edge conduction in monolayer WTe_2.*Nat. Phys.* **13**, 677–682 (2017).
18. Wu, S. et al. Observation of the quantum spin Hall effect up to 100 kelvin in a monolayer crystal. *Science* **359**, 76–79 (2018).
19. Fei, Z. et al. Ferroelectric switching of a two-dimensional metal. *Nature* **560**, 336–339 (2018).
20. Sajadi, E. et al. Gate-induced superconductivity in a monolayer topological insulator. *Science* **362**, 922–925 (2018).
21. Fatemi, V. et al. Electrically tunable low density superconductivity in a monolayer topological insulator. *Science* **362**, 926–929 (2018).
22. Ma, Q. et al. Observation of the nonlinear Hall effect under time-reversal-symmetric conditions. *Nature* **565**, 337–342 (2019).
23. Luo, Y. et al. Hall effect in the extremely large magnetoresistance semimetal WTe_2. *Appl. Phys. Lett.* **107**, 182411 (2015).
24. Olbrich, P. et al. Room-temperature high-frequency transport of Dirac fermions in epitaxially grown Sb_2Te_3- and Bi_2Te_3-based topological insulators. *Phys. Rev. Lett.* **113**, 096601 (2014).
25. Yu, H., Wu, Y., Liu, G.-B., Xu, X. & Yao, W. Nonlinear valley and spin currents from Fermi pocket anisotropy in 2D crystals. *Phys. Rev. Lett.* **113**, 156603 (2014).
26. Edelstein, V. M. Spin polarization of conduction electrons induced by electric current in two-dimensional asymmetric electron systems. *Solid State Commun.* **73**, 233–235 (1990).
27. Lee, J., Wang, Z., Xie, H., Mak, K. F. & Shan, J. Valley magnetoelectricity in single-layer MoS_2. *Nat. Mater.* **16**, 887–891 (2017).
28. Mak, K. F., Xiao, D. & Shan, J. Light–valley interactions in 2D semiconductors. *Nat. Photon.* **12**, 451–460 (2018).
29. MacNeill, D. et al. Control of spin–orbit torques through crystal symmetry in WTe_2/ferromagnet bilayers. *Nat. Phys.* **13**, 300–305 (2016).
30. MacNeill, D. et al. Thickness dependence of spin–orbit torques generated by WTe_2. *Phys. Rev. B* **96**, 054450 (2017).
31. Tian, Y., Ye, L. & Jin, X. Proper scaling of the anomalous Hall effect. *Phys. Rev. Lett.* **103**, 087206 (2009).
32. Ye, L. et al. Massive Dirac fermions in a ferromagnetic kagome metal. *Nature* **555**, 638–642 (2018).
33. Xu, S.-Y. et al. Electrically switchable Berry curvature dipole in the monolayer topological insulator WTe_2. *Nat. Phys.* **14**, 900–906 (2018).

Acknowledgements

The research was supported by ARO Award W911NF-17-1-0605 for sample fabrication and transport measurements, and the US Department of Energy, Office of Basic Energy Sciences under award no. DESC0013883 for optical measurements. It was also partially supported by the Cornell Center for Materials Research with funding from the NSF MRSEC program (DMR-1719875) for the low-temperature studies. This work was performed in part at Cornell NanoScale Facility, an NNCI member supported by NSF Grant NNCI-1542081. We also thank the David and Lucille Packard Fellowship and a Sloan Fellowship (K.F.M.) for support and G. Stiehl for fruitful discussions on the crystal symmetry properties of multilayer T_d-WTe_2.

Author contributions

K.K. and T.L. fabricated the devices. E.S., T.L. and K.K. developed the experimental set-up and performed the measurements. K.K., T.L. and K.F.M. analysed the data. J.S. and K.F.M. developed the model and wrote the paper. All the authors discussed the results and commented on the manuscript.

Competing interests
The authors declare no competing interests.

Additional information
Supplementary information is available for this paper at https://doi.org/10.1038/s41563-019-0294-7.

Reprints and permissions information is available at www.nature.com/reprints.

Correspondence and requests for materials should be addressed to J.S. or K.F.M.

Methods

Sample and device fabrication. Van der Waals heterostructures of few-layer WTe_2 and hexagonal boron nitride (hBN) were fabricated by the layer-by-layer dry transfer method[34]. In this process, few-layer WTe_2 and hBN were mechanically exfoliated from bulk crystals (HQ Graphene) onto silicon substrates. The hBN and WTe_2 flakes were picked up by a stamp consisting of a thin film of polycarbonate on polydimethylsiloxane. The stack was then released onto a Si substrate with prepatterned Pt electrodes. To prevent sample degradation, the exfoliation and transfer processes were performed in a nitrogen-filled glovebox.

The thickness of WTe_2 layers was first estimated by optical contrast, and then measured by atomic force microscopy after device fabrication. The crystal orientation of WTe_2 flakes was inferred from the polarized Raman spectroscopy[10]. To avoid geometrical complications on the current path, rectangular strips were chosen for the Hall bar devices. The crystal *a*-axis was aligned parallel to the electrodes for current injection. For the disc devices, the crystal *a*-axis was aligned with one of the 16 Pt electrodes. The WTe_2/hBN stacks were patterned into a circular shape using a mask that is made of e-beam-exposed poly(methylmethacrylate) (PMMA) A4/PMMA M2 bilayers followed by reactive ion etching using SF_6 gas. The devices were subsequently left in acetone for 30 min to remove the PMMA residues.

Linear and nonlinear transport measurements. The transport measurements were carried out in a Quantum Design Physical Property Measurement System (PPMS) and an Oxford Teslatron system down to 1.8 K. A harmonic current was applied to the devices. The longitudinal and transverse voltage drops were measured at the fundamental and the second-harmonic frequencies with lock-in amplifiers. The d.c. component was measured with a voltmeter. The longitudinal resistivity of the Hall bar devices was obtained as $\rho_{\parallel}=\frac{V_{\parallel}}{I}\frac{L_{\perp}d}{L_{\parallel}}$, where $L_{\parallel}$ and $L_{\perp}$ are the longitudinal and transverse dimensions of the Hall bar device, respectively, and d is the sample thickness. Similarly, $\rho_{\perp}$ was obtained by using $V_{\perp}$ in place of $V_{\parallel}$. The longitudinal conductivity is related to the resistivity by $\sigma=1/\rho_{\parallel}$.

The angular dependence of the nonlinear AHE was measured in disc devices in a rotating reference frame (source–A–drain–B in a clockwise sequence) following the Hall measurement convention (Fig. 2b). Current was injected from the source to the drain electrodes. A and B were the high and low inputs of a voltmeter or lock-in amplifier, respectively. When the source and drain contacts were reversed to switch the bias current direction, the Hall probe electrodes (A and B) were also switched. The sign of the Hall voltage follows the sign of the current-induced magnetization. To extract the angular dependence of the nonlinear AHE in disc devices, $V_{\perp}^{2\omega}$ for a given θ was first antisymmetrized between two opposing current directions, that is $[V_{\perp}^{2\omega}(\theta)-V_{\perp}^{2\omega}(\theta+180^{\circ})]/2$. Antisymmetrization is generally needed because of the longitudinal–transverse coupling. It is not needed for current along the high-symmetry axes.

Angular dependence of the second-order nonlinear response. The second-order nonlinear current density $\mathbf{j}^{(2)}$ in response to an electric field $\mathbf{E}$ in a material can be expressed through the material's second-order nonlinear susceptibility $\chi^{(2)}$ as $\mathbf{j}^{(2)}=\chi^{(2)}\cdot\mathbf{E}\cdot\mathbf{E}$ (refs. [3,8]). For few-layer T_d-WTe_2 with Pm point group symmetry, the nonlinear susceptibility has 10 non-zero independent elements d_{ij} as shown below:

$$\chi^{(2)}=2\begin{pmatrix} d_{11} & d_{12} & d_{13} & 0 & d_{15} & 0\\ 0 & 0 & 0 & d_{24} & 0 & d_{26}\\ d_{31} & d_{32} & d_{33} & 0 & d_{35} & 0\end{pmatrix} \tag{3}$$

Coordinates x, y and z are chosen along the principal axes of the crystal, namely, parallel to the mirror line (*b*-axis), perpendicular to the mirror line in the plane (*a*-axis) and perpendicular to the plane (*c*-axis), respectively. For an in-plane electric field $\mathbf{E}=(E_x,E_y,0)$, the nonlinear current density $\mathbf{j}^{(2)}$ is given as

$$\mathbf{j}^{(2)}=\begin{pmatrix} d_{11}E_x^2+d_{12}E_y^2\\ 2d_{26}E_xE_y\\ d_{31}E_x^2+d_{32}E_y^2\end{pmatrix} \tag{4}$$

Next we obtain the second-order nonlinear electric field $\mathbf{E}^{(2)}$ from $\mathbf{j}^{(2)}$ by using the Ohm's law $\mathbf{E}^{(2)}=\rho\cdot\mathbf{j}^{(2)}$, where $\rho=\begin{pmatrix}\rho_b & 0 & 0\\ 0 & \rho_a & 0\\ 0 & 0 & \rho_c\end{pmatrix}$ is the resistivity tensor for anisotropic WTe_2. The two in-plane components of $\mathbf{E}^{(2)}$ are $\begin{pmatrix}\rho_b(d_{11}E_x^2+d_{12}E_y^2)\\ 2\rho_a d_{26}E_xE_y\end{pmatrix}$.

We derive equation (1) for an in-plane bias current $\mathbf{j}=j\begin{pmatrix}\cos\theta\\ \sin\theta\end{pmatrix}$ of amplitude j and angle θ measured from the mirror line (*x*-axis). The first-order electric field from Ohm's law is $\mathbf{E}=j\begin{pmatrix}\rho_b\cos\theta\\ \rho_a\sin\theta\end{pmatrix}$. The longitudinal component, that is the component parallel to $\mathbf{j}$, is $E_{\parallel}=j(\rho_b\cos^2\theta+\rho_a\sin^2\theta)$. On the other hand, the transverse component of the second-order electric field, that is the in-plane component perpendicular to $\mathbf{j}$, is $E_{\perp}^{(2)}=j^2\rho_b^3\sin\theta\,[d_{12}r^2\sin^2\theta+(d_{11}-2d_{26}r^2)\cos^2\theta]$, where r is the resistivity anisotropy defined as $r\equiv\frac{\rho_a}{\rho_b}$. One can thus obtain

$$\frac{E_{\perp}^{(2)}}{(E_{\parallel})^2}=\frac{\rho_b\sin\theta\,[d_{12}r^2\sin^2\theta+(d_{11}-2d_{26}r^2)\cos^2\theta]}{(\cos^2\theta+r\sin^2\theta)^2} \tag{5}$$

Equation (5), equivalent to equation (1), describes well the experimental angular dependence of the nonlinear AHE shown in Fig. 3c. The largest nonlinear Hall response occurs at $\theta=90^{\circ}$, at which $\frac{E_{\perp}^{(2)}}{(E_{\parallel})^2}=\rho_b d_{12}$ and $\sigma_{\mathrm{AH}}=d_{12}E_{\parallel}$.

Estimate of the Berry curvature dipole and the current-induced magnetization. In the low-frequency limit, as in our experiment, the intrinsic contribution to the nonlinear Hall conductivity $\sigma_{\mathrm{AH}}\approx\frac{\pi}{2}\frac{kG_0}{d}D$ can be expressed through the Berry curvature dipole D (ref. [3]). In two dimensions, it has the dimension of length. Here G_0 is the conductance quantum and $\hbar k\equiv eE_{\parallel}\tau$ is the net electronic momentum gained under an in-plane bias $E_{\parallel}$ ($\hbar$ and e denote, respectively, the Planck constant and elementary charge). On the other hand, the longitudinal conductivity can be expressed as $\sigma=G_0v_{\mathrm{F}}k_{\mathrm{F}}\tau/2d$, where v_{F} and k_{F} are the Fermi velocity and Fermi vector, respectively, and are related to the Fermi energy as $\epsilon_{\mathrm{F}}\sim\hbar v_{\mathrm{F}}k_{\mathrm{F}}$. We thus obtain $\frac{\sigma_{\mathrm{AH}}}{\sigma E_{\parallel}}\approx\frac{\pi D}{(\hbar v_{\mathrm{F}}k_{\mathrm{F}})/e}\sim\frac{\pi D}{\epsilon_{\mathrm{F}}/e}$. Based on this relation, the Berry curvature dipole D was evaluated from the experimental value of $\frac{\sigma_{\mathrm{AH}}}{\sigma E_{\parallel}}$ in the limit of $\sigma\to0$ if the intrinsic effect dominates the nonlinear Hall conductivity. Here we used $\epsilon_{\mathrm{F}}\sim50$ meV from ab initio band structure calculations of bulk crystals[11,35]. (Note that atomically thin samples are likely to have a smaller Fermi energy due to quantum confinement[15].) We can also estimate the current-induced magnetization $M\sim j\times D$ (refs. [3,27]). For a typical current density of $j\sim10\,\mathrm{A\,m^{-1}}$ from the experiment and Berry curvature dipole of $D\sim1$ Å[33], we obtain a current-induced magnetization of $M\sim1$ nA. The value corresponds roughly to one Bohr magneton in a thousand charge carriers in 2D WTe_2 (with a sheet carrier density of $\sim10^{13}\,\mathrm{cm^{-2}}$).

Data availability

The data supporting the plots within this paper and other findings of this study are available from the corresponding authors upon request.

References

34. Wang, L. et al. One-dimensional electrical contact to a two-dimensional material. *Science* **342**, 614–617 (2013).
35. Chang, T.-R. et al. Prediction of an arc-tunable Weyl Fermion metallic state in $Mo_xW_{1-x}Te_2$. *Nat. Commun.* **7**, 10639 (2016).